Larmor precession: observation and utilization for boosting the signal intensity of radio frequency glow discharge mass spectrometry

Article (Accepted Version)

Larmor Precession: Observation and Utilization for Boosting the Signal Intensity of Radio Frequency Glow Discharge Mass Spectrometry

Mengli Wang,[†, ‡, ⊥] Rong Qian,[*, †, ⊥] Shangjun Zhuo,[†, ‖, ⊥] Qiao Chen,[§] Zhongquan Li,[†] Bin Zhao[‡]

[†] National Center for Inorganic Mass Spectrometry in Shanghai, Shanghai Institute of Ceramics, Chinese Academy of Sciences, 1295 Ding Xi Road, Shanghai 200050, People's Republic of China

[‡] School of Material Science and Engineering, University of Shanghai for Science and Technology, 516 Jungong Road, Shanghai 200093, People's Republic of China

[§] Department of Chemistry, School of Life Sciences, University of Sussex, Brighton BN1 9QJ, United Kingdom

[‖] State Key Laboratory of High Performance Ceramics and Superfine Microstructures, Shanghai Institute of Ceramics, Chinese Academy of Sciences, 1295 Ding Xi Road, Shanghai 200050, People's Republic of China

[⊥] Center of Materials Science and Optoelectronics Engineering, University of Chinese Academy of Sciences, 19(A) Yuquan Road, Beijing, People's Republic of China

* E-mail: qianrong@mail.sic.ac.cn

KEYWORDS: Larmor precession, rf-GD-MS, magnet array, signal intensity, enhancement

ABSTRACT: A novel magnet array system was constructed to use Larmor precession for boosting the signal intensity of rf-GD-MS. The enhancement mechanism with four magnet array devices of single block magnet and 2×2, 3×2, and 3×4 magnet arrays was simulated and studied by COMSOL Multiphysics Software 5.4.0 (COMSOL) to determine if the electrons in the discharge plasma could perform Larmor precession along the direction perpendicular to the magnetic field. Induced by Larmor precession, inelastic collisions between the primary electrons and sample produced numerous secondary electrons and further improved the ionization efficiency. Moreover, the fuzzy synthetic evaluation result predicted that the device with 3×2 magnet array would display the greatest enhancement effect among the four devices. Based on these theoretical studies, a magnet array system with four magnet array devices was fabricated and utilized for studies of two scintillation crystals BGO and PWO. The observations indicated that the signal intensities obtained for ^{209}Bi and ^{208}Pb with the magnet array system were 630-3600 times of that obtained without magnet, and were enhanced by a factor of 1.5-2.8 compared with a previously reported stacked magnetic device. Two NIST samples were used to validate the method, and the results suggested that relative errors were less than 10% and the lowest detection limit for the 3×2 magnet array could reach 0.0032μg·g^{-1}. Furthermore, the magnet array enhancement system with Larmor precession offers an efficient and sensitive approach for the direct analysis of non-conducting materials.

INTRODUCTION

The rapid development of new inorganic materials and the effect of trace elements on material properties has increased the need for more facile and efficient techniques for characterization.[1, 2] Glow discharge mass spectrometry (GD-MS) is often the best choice for the direct analysis of solid materials because it generates a stable analyte ion population directly and avoids the problems of dissolution, dilution, and contamination that may arise from techniques requiring solution samples.[3-7] The ability to analyze solids directly, and the ease of preparation, low detection limit (down to ng·g^{-1}) and minimal matrix effects have made GD-MS useful for accurate determination of trace and ultra-trace elements in solid materials.[8-12]

Although GD-MS has been widely used in advanced materials, geology, environmental science, and other fields, it usually requires conducting material to support the discharge of the insulators because of poor sample conductivity.[13-18] The introduction of a radio-frequency (rf) source into GD-MS allows direct analysis of conductive and non-conductive samples, either bulk solids or layered materials. In addition, the development of a pulsed-rf-GD source has improved the analytical capabilities of rf-GD techniques. Bouza et al. applied rf-PGD-TOFMS for the determination of compositional depth profiles of coated glasses to differentiate element concentrations for the different layers of the samples.[19] Bodnar et al. designed a GD-TOF-MS quantification method for effective ionization of the elements in insoluble crystal materials with fluorine-doped potassium titanyl phosphate (KTP) $KTiOPO_4$:KF.[20] Fernandez et al. used rf-PGD-TOFMS for depth profiling analysis of perovskite absorber layers with different synthetic precursors (PbI_2, $PbCl_2$ and $PbBr_2$).[21] These techniques further broadened

the application of GD-MS for the direct analysis of non-conductive samples significantly.

In the glow discharge process, samples can be sputtered and ionized directly when GD-MS is equipped with a rf source.[22] For over four decades, many efforts have been concentrated on improving the analytical capability for the rf-GD spectrometries.[17, 23-28] Moreover, there are still many development possibilities for both techniques and applications even if rf-GD-MS has also been proved for the analysis of non-conducting samples as well as for depth profile analysis. Bentz et al. studied a modified cathode ion source with a magnetic field to increase the ionization efficiency.[23] Hentz et al. reported a rf planar magnetron GD source to produce effective emission signal, precession and detection limit.[25] Vega et al. designed a compact magnetically-boosted rf glow discharge coupled to a mass spectrometer to enhance signal intensities.[27] Recently, our group constructed a stacked magnetic system for rf-GD-MS to enhance the signal intensities for the analyte ions. A possible enhancement mechanism was also proposed with stacked magnets producing an oscillating magnetic distribution to extend the path of electrons and increase ionization efficiency.[28]

The added external magnetic field and resulting Lorentz forces put the charged particles into a spiral trajectory, resulting in increased ion bombardment probability for higher sputtering rates and signal intensities. This enhancement was evidently affected by the magnetic field strength and its spatial distribution. Under the action of the Lorentz force, the electron can change course and move in a direction perpendicular to the magnetic induction line and velocity, generating Larmor precession.[29-31] Moreover, the Larmor Precession trajectory is related to the magnitude and direction of the Lorentz force. The larger the Lorentz force and the more complex the direction, the longer the precession trajectory will be.

In the present work, a novel magnet array system was constructed with Larmor precession and applied into rf-GD-MS. The enhancement mechanism of the system was systematically studied with COMSOL and fuzzy synthetic evaluation methods. Then, four magnetic devices with single block and 2×2, 3×2, and 3×4 magnet arrays were fabricated. Furthermore, the stability, accuracy, and detection limit were verified with two NIST samples and two crystals. In addition, the theoretical studies suggested that the electrons in the discharge plasma in the array magnetic enhancement rf-GD-MS system could conduct Larmor precession, which might contribute to an increase in the ionization efficiency.

EXPERIMENTAL SECTION

2.1 Simulations of the Magnetic Flux Density and the Motions of Electrons and Argon Ions by COMSOL Method

In order to observe and compare the effects of the magnet array devices vs. the device without magnet, the magnetic flux density and the motions of electrons and Ar^+ ions were simulated and studied by COMSOL Multiphysics Software 5.4.0 (COMSOL). Four theoretical models of magnet array devices with a single block magnet (20 mm × 15 mm × 5 mm), 2×2 (10 mm ×7.5 mm ×5 mm for each piece), 3×2 (10 mm × 5 mm ×5 mm for each piece) and 3×4 (5 mm ×5 mm ×5 mm for each piece) magnet arrays were constructed for COMSOL studies. The typical NdFeB magnet was selected for this study with a magnetic permeability of 1.05 and coercivity of 876 kA/m. Considering stacking of the magnetic blocks could lead to degaussing and loss of magnetic field strength, two arrangement modes were simulated with small magnetic blocks inside a copper shell including the arrangements with magnets stacked as in our previous work[27] or separated by the support materials.

The magnetic flux density was calculated in the COMSOL AC/DC module, and the motions of the charged particles were simulated in the Charged Particle Tracing module with an electric field applied. The static magnetic field distribution was simulated with the mode "magnetic field, no current (mfnc)," and the governing equations for the magnetic field are shown in Eqs 1 and 2. The governing equation for tracing the motions of charged particles is shown was also showed in Eq 3. After optimization of the values of the mass, velocity and position of the incident particles, the motions of electrons and Ar^+ particles in the glow discharge process were simulated and investigated.

$$\mathbf{H} = -\nabla V_m \quad (1)$$

$$\nabla \cdot \mathbf{B} = 0 \quad (2)$$

$$\frac{\mathrm{d}(m_p\ \mathrm{v})}{\mathrm{dt}} = \mathbf{F}_t \quad (3)$$

Here, **H** is the magnetic field intensity, ∇ is the vector differential operator that represents the rate of change of the field in space, V_m is the velocity of the charged particle, **B** is the magnetic flux density, m_p is the mass of charged particle, dt represents the time of motion of charged particle, and $\mathbf{F_t}$ is the force on the charged particle.

2.2 Construction of Magnet Array System

For the rf-GD-MS investigation experiments, a magnet array system of rf-GD-MS was designed and fabricated by using a copper shell (6 mm in height and 28 mm in diameter) containing the magnetic blocks inside. The magnetic device was placed on the back of the analyte sample in the rf-GD-MS discharge chamber. The magnet utilized in this study was the NdFeB magnet with a permeability of 1.05 and coercivity of 876 kA/m. Then, four types of the magnet array devices with magnet array stacked and separated, including the single block magnet (20 mm × 15 mm × 5 mm), 2×2 (10 mm ×7.5 mm ×5 mm for each piece), 3×2 (10 mm × 5 mm ×5 mm for each piece) and 3×4 (5 mm ×5 mm ×5 mm for each piece) magnet arrays, were respectively placed into the magnetic devices. The arrangements of magnets in the copper shells are shown in Figure 1 and Figure 2. The magnetic field of the transverse block magnet and transverse array magnets were parallel to the sample surface and perpendicular to the electric field.

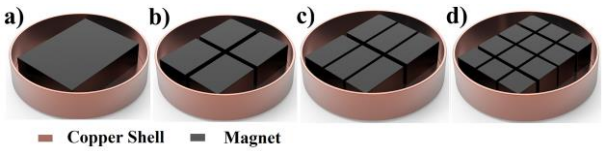

Figure 1. Diagram of four rf-GD-MS magnetic devices with transverse magnet array stacked: (a) single magnet, (b) 2×2

magnet array, (c) 3×2 magnet array and (d) 3×4 magnet array.

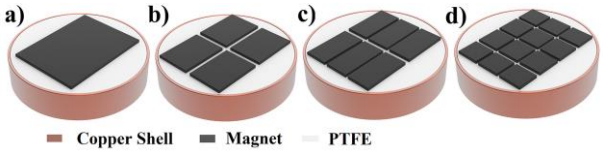

Figure 2. Diagram of four rf-GD-MS magnetic devices with transverse magnet array separated by PTFE: (a) single magnet, (b) 2×2 magnet array, (c) 3×2 magnet array and (d) 3×4 magnet array.

2.3 Materials and Sample Preparation

To investigate the performance of the rf-GD-MS magnet array system, two crystals were analyzed in the present work. $Bi_4Ge_3O_{12}$ (BGO) doped with Mg, Al, Si, Cr and PWO_4 (PWO) doped with Al, K, P, Fe were provided by Shanghai Institute of Ceramics, Chinese Academy of Sciences. For further validation of the magnetic system, two NIST standard reference materials, SRM 611 and SRM 612 were used. Before the rf-GD-MS experiment, all the samples were cleaned with dilute nitric acid solution and deionized water. Then, the samples were preserved in anhydrous ethanol prior to the experiments.

2.4 rf-GD-MS Experiments

The rf-GD-MS experiments were performed with an Auto Concept GD 90 radio-frequency glow discharge mass spectrometry (Mass Spectrometry Instruments Ltd., U.K.) with a double focusing Nier-Johson forward geometry configuration with a minimal system. The ion source consists of a chamber with anode potential and the sample inside the sample holder functioning as cathode (Figure 3). The sample holder was modified to include a spring loaded cylindrical magnetic device that has a flat seat to adapt a flat sample. The rf-power was directly applied onto the magnetic device through an electrical probe. High-purity argon gas (> 99.9999%) was injected into the source chamber with controlled flow rates.

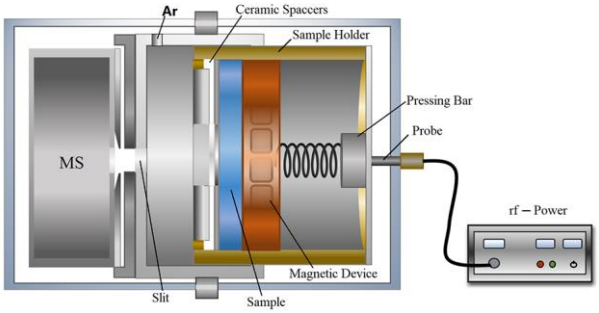

Figure 3. Diagram of Discharge Chamber of the rf-GD-MS.

The rf-GD-MS experiments were carried out with the discharge pressure in the range of 2.0-8.5 mPa and rf-power in the range of 20-60 W. The ion source was precooled with liquid nitrogen to reduce contamination from C, N, and O elements. All major/high intensity peaks (above 10^{-13} A) were measured with a Faraday detector, and the low intensity peaks (below 10^{-13} A) were measured with an ion counter with a channeltron. The working resolution of about 4000 was used for most of the measurements.

RESULTS AND DISCUSSION

3.1 Theoretical Simulation and Studies on Enhancement Mechanism of the rf-GD-MS with Magnet Array System

3.1.1 Simulation of Magnetic Flux Density of the Magnet Array System

In initial theoretical studies, the magnetic flux density and field distribution for the magnet arrays were simulated. In the case of the array magnets stacked to each other (Figure 1), it was worth noting that no apparent magnetic flux was observed for 2×2, 3×2, or 3×4 magnet arrays by COMSOL studies. Hence, some polytetrafluoroethylene (PTFE) grids were constructed and placed in the copper shell first, and the magnet blocks were inserted into the grids for separation (Figure 2).

The simulation results for magnetic flux density suggested that the four magnetic modes could display distinct oscillating magnetic field distributions. As shown in Figure 4a, the magnetic flux density of the single block magnet displayed a broad peak with maximum density 0.22 T, the 2×2 magnet array displayed two peaks with maximum density 0.11 T, the 3×2 magnet array displayed two peaks with maximum density 0.20 T, and the 3×4 magnet array displayed four peaks with maximum density 0.20 T. Figures 4b-e show the distributions of the magnetic fields around the magnets, and different magnetic field strengths and oscillating peaks are expected to play different roles in regulating the movement of electrons.

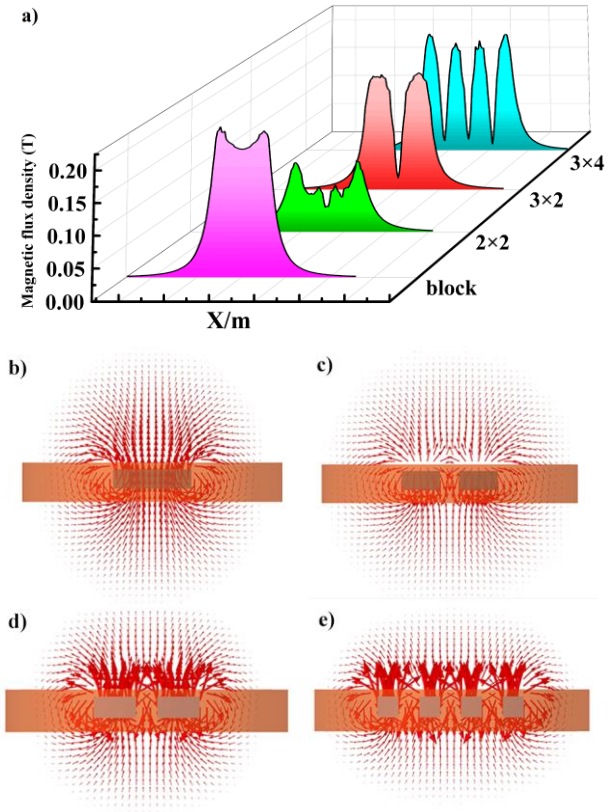

Figure 4. COMSOL simulation of (a) magnetic flux density and magnetic field distribution of (b) single block magnet, (c) 2×2 magnet array, (d) 3×2 magnet array and (e) 3×4 magnet array.

3.1.2 Investigation on Larmor Precession of Electrons

In general, the effect of a magnetic field on a glow discharge is due to the electrons; at the fields customarily used, the ions are influenced insignificantly. The lifetime of an electron in the discharge can be prolonged by using a magnetic field to redirect electron motion in a manner that extends the net electron path length.[25] In the glow discharge process, the electrons usually play a critical role in sputtering and ionization processes. Therefore, the contributions of the electrons in the plasma were first investigated with COMSOL for the rf-GD-MS magnet array system. Without the applied magnets, the motion of an electron resembled a linear path when they impacted and then left the sample surface (Figure 5a). With the single block and 2×2, 3×2, and 3×4 magnet arrays (Figures 5b-e), the electron trajectories were curved and they spun near the sample surface, which would cause inelastic collisions between primary electrons and sample to produce numerous secondary electrons (Dynamic simulation is illustrated in the Supporting Information S1). The investigations of different electron motions further suggest that the movements of high-speed electrons perpendicular to the magnetic induction line were considered as the Larmor precession induced by Lorentz forces (Figure 5f). [29-31]

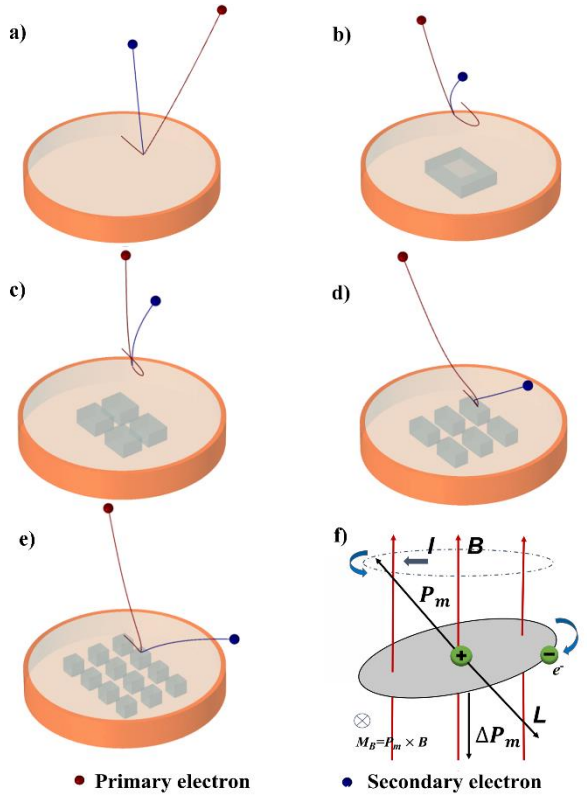

Figure 5. COMSOL simulation of single electron motion on the surface of sample under the influence of magnetic devices: (a) no magnet, (b) single block, (c) 2×2 magnet array, (d) 3×2 magnet array, (e) 3×4 magnet array and (f) diagram of Larmor precession.

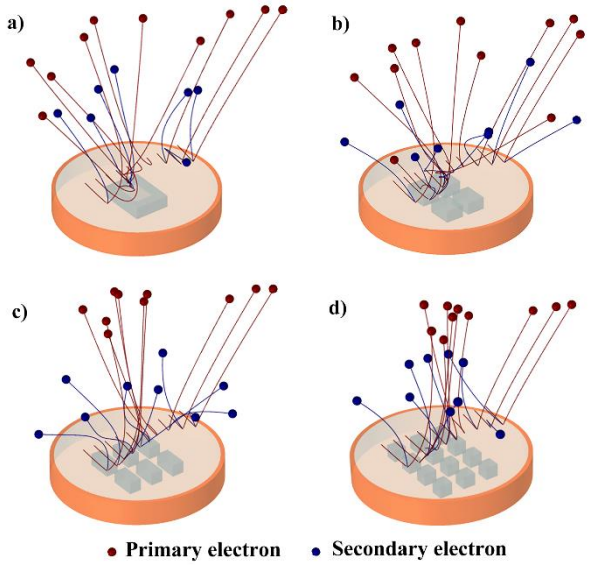

Figure 6. COMSOL simulation of multiple electrons motions on the sample surface under the influence of magnetic devices: (a) single block with 7 secondary electrons obtained, (b) 2×2 magnet array with 8 secondary electrons obtained, (c) 3×2 magnet array with 9 secondary electrons obtained and (d) 3×4 magnet array with 9 secondary electrons obtained.

With Larmor precession, the spiral path of the electron and the path duration time could be extended in the discharge area. In addition, Larmor precession produced many secondary electrons resulting from inelastic collisions of primary electrons and samples, leading to more collisions between electrons and other particles and increases in the sputtering rate and the ionization efficiency. Moreover, Figure 6 indicates that electrons moved in four different trajectories with the four magnet array devices, thereby producing different numbers of secondary electrons while the number of primary electrons was 10 (Dynamic simulation is illustrated in the Supporting Information S2). This distinction can be attributed to the influence on the Larmor precession trajectory exerted by different magnetic field distributions in the four magnet array devices. Hence, the probabilities and degrees of deflection of the electron trajectories by four magnet array devices were also different, which would produce dissimilar enhancements of the signal intensities.

3.1.3 Investigation on Ar^+ Motions in Discharge Processes

The behavior of Ar^+ ions in the glow discharge process in the rf-GD-MS magnet array system was also investigated, and this suggested that the Lorentz force also affected the motions of argon ions. As shown in Figure 7, the trajectories of Ar^+ ions varied with the distribution of the magnetic field, and the trajectories were distinctly curved; they ultimately produced many electrons, and this differed from the single trajectory seen without a magnet (Dynamic simulation is illustrated in the Supporting Information S3). Although the magnetic array system might extend the trajectories of Ar^+ and cause more collisions between Ar^+ and other particles, no apparent differences were observed between the single block and 2×2, 3×2, and 3×4 magnet arrays.

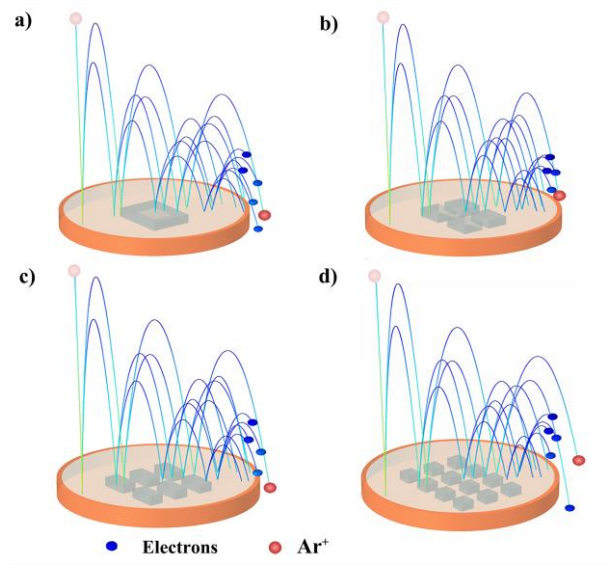

Figure 7. COMSOL simulation of Ar^+ motion on the sample surface under the influence of magnetic devices: (a) single block, (b) 2×2 magnet array, (c) 3×2 magnet array and (d) 3×4 magnet array.

Moreover, the mass of Ar^+ and electron are 6.64×10^{-26} kg and 9.11×10^{-31} kg, and they have the same charge of one elementary charge. Under the same electric field and magnetic field, both Ar^+ and electron could be driven by identical electric forces and Lorenz forces. For the mass of electron was much smaller than Ar^+, the trajectories of electrons could be affected much more intense than Ar^+ by magnetic field. For the same distance, the time required for Ar^+ is much longer than that required for the electron. Hence, the enhancement of Ar^+ motion is not expected to be as effective as that of the electrons. However, the motions of Ar^+ in the array magnetic field could also produce some electrons to engage in Larmor precession.

3.1.4 Evaluation of Enhancement Effects with the Fuzzy Synthetic Evaluation Method

To evaluate the enhancement effects for the four magnet array devices, a fuzzy synthetic evaluation method (FSEM) was utilized.[32] Combined with the theoretical studies, five evaluation factors were selected to evaluate the effects, including M_1 related to the magnetic flux density, M_2 related to the magnetic field oscillation peaks, M_3 related to probability of secondary electron sputtering, M_4 related to the probability of deflected electrons and M_5 related to the deflection amplitude for an electron's trajectory.

Table 1 Enhancement Factors and Evaluation Results (W) for Four Magnet Arrays by FSEM

factors	single block	2×2 magnet array	3×2 magnet array	3×4 magnet array	weight
M_1	1	0.5	0.91	0.91	0.1
M_2	0.25	0.5	0.5	1	0.1
M_3	7/10	8/10	9/10	9/10	0.3
M_4	14/17	12/18	16/19	13/19	0.2
M_5	0.5	0.8	0.6	0.4	0.3
W	0.65	0.71	0.76	0.72	-

During the normalizing process, M_1 and M_2 were defined with an extreme value method for dimensionless treatment of the original data as Eq 1. M_3 was the ratio of secondary electrons to the number of primary electrons (Figure 6), M_4 was the ratio of the number of the deflected electrons to the total electrons, and M_5 was defined by fuzzy mathematics, according to the angle and degree of deflection, as a value between 0 and 1 (0.5 for block magnet, 0.8 for 2×2 array, 0.6 for 3×2 array and 0.4 for 3×4 array). The weights of the five factors were determined by COMSOL simulations, the evaluation value P_i for each factor was calculated with Eq 5, and the comprehensive evaluation result (***W***) was obtained with Eq 6.

$$\boldsymbol{M_i} = \frac{\boldsymbol{x_j} - \min \boldsymbol{x_j}}{\max \boldsymbol{x_j} - \min \boldsymbol{x_j}} (i = 1, 2,\ 1 \le j \le n) \quad (4)$$

$$\boldsymbol{W} = \sum \boldsymbol{P_i} = \sum \boldsymbol{M_i} \times \boldsymbol{\lambda_i}\ (i = 1, 2, 3, 4, 5) \quad (5)$$

$$\boldsymbol{W} = 0.1\times\boldsymbol{M_1} + 0.1\times\boldsymbol{M_2} + 0.3\times\boldsymbol{M_3} + 0.2\times\boldsymbol{M_4} + 0.3\times\boldsymbol{M_5} \quad (6)$$

In Eq 1, $\boldsymbol{x_j}$ is the value of magnetic flux density (Figure 4) when j = 1, $\boldsymbol{x_j}$ is the number of magnetic field oscillation peaks (Figure 4) when j = 2, $\min x_j$ is 0 in the case of no magnet and $\max x_j$ is the maximum value for the original magnetic flux density or the number of magnetic field oscillation peaks. In Eq 2, $\boldsymbol{M_i}$ is the value of factor i, and $\boldsymbol{\lambda_i}$ is the weight of factor i. Then, the evaluation results for the four magnet array devices were calculated as 0.65, 0.71, 0.76, and 0.72 (Table 1). Obviously, the results estimate that the enhancement effect of the 3×2 magnet array is better than those of the other three devices, which could provide some significant guidance for future design of the magnetic array system and the rf-GD-MS experiments.

3.2 Fabrication of the Magnet Array System and Investigation on the Influences of the Parameters of rf-GD-MS and Arrangement of Magnet Arrays

Based on the theoretical studies, a magnet array system was fabricated for Larmor precession and applied into rf-GD-MS. The four magnetic devices with single block magnet and 2×2, 3×2, and 3×4 magnet arrays separated by PTFE grids were utilized for the investigations (Figure 2). For rf-GD-MS experiments, the discharge pressure and rf-power have been reported to possibly affect the ionization efficiency. Here, two non-conducting samples of BGO and PWO were utilized to demonstrate the influences of the magnetic field strength under different conditions, including the four magnet array devices, the discharge pressure and the rf-power.

3.2.1 Optimization of rf-GD-MS Parameters for Signal Enhancement with the Magnet Array System

The discharge dependence of magnetic enhancement is shown in Figure 7. The relationship between discharge pressure and signal intensity was examined with the single block and 2×2, 3×2 and 3×4 magnet arrays. The discharge pressure was optimized from 2.0 mPa up to 8.5 mPa and rf-power was fixed at 50 W. As shown in Figure 8, the signal intensities gradually increased with increasing discharge pressure; the increased discharge pressure meant more argon ions were excited and the

probability of sputtering the solid sample increased. With the magnet array system, such an increase was suggested to play a synergetic enhancement effect in the rf-GD-MS signal intensity.

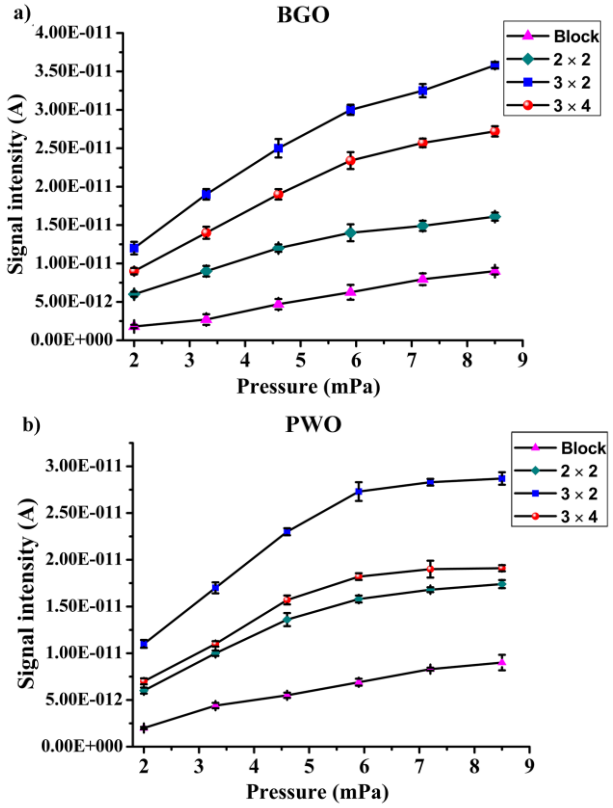

Figure 8. rf-GD-MS intensity of (a) matrix element ^{209}Bi (67.1 wt%) in BGO, (b) matrix element ^{208}Pb (45.5 wt%) in PWO, as a function of discharge pressure with constant rf-power of 50 W and single block and 2×2, 3×2 and 3×4 magnet arrays.

The rf-power dependence magnetic enhancement was performed using BGO and PWO with rf-power ranging from 20 to 60 W while the discharge pressure was fixed at 5.9 mPa. Figure 9 shows that the signal intensities increased with increasing rf-power in the range of 20-60 W; increased rf-power could increase the density and kinetic energy of ions, which improved the sputtering and ionization efficiency. Moreover, the signal intensity was increased further by the utilization of magnetic devices. However, high rf-power might lead to fragmentation of crystal samples, which might be caused by the poor heat conduction of the non-conducting samples.[28] Therefore, the discharge pressure and rf-power were optimized and fixed at 5.9 mPa and 50 W for the following investigations.

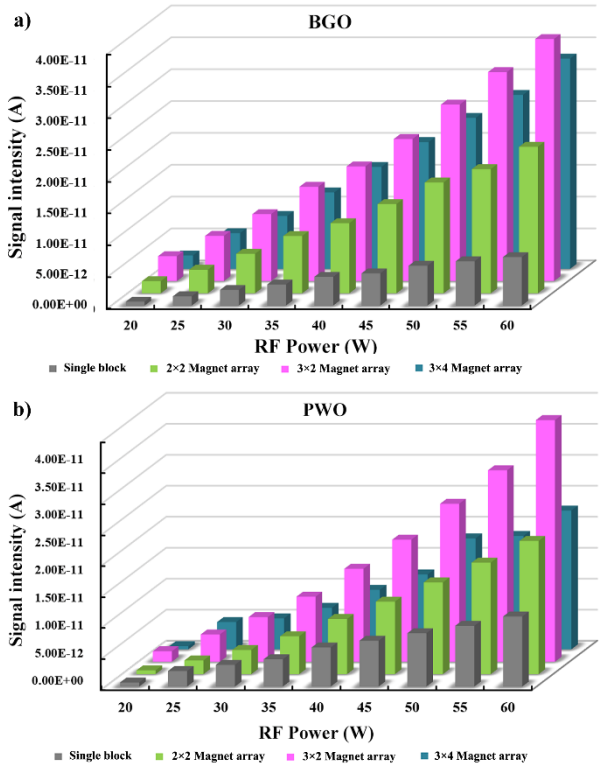

Figure 9. rf-GD-MS intensity of (a) ^{209}Bi (67.1 wt%) in BGO, (b) ^{208}Pb (45.5 wt%) in PWO, as a function of rf-power at the discharge pressure of 5.9 mPa and the single block, 2×2, 3×2 and 3×4 magnet arrays.

3.2.2 Investigation on the Influence of the Arrangement of Magnet Arrays

To further investigate the effect of the arrangement of the magnet array on signal enhancement, rf-GD-MS experiments with a single block and 2×2, 3×2 and 3×4 magnet arrays were utilized to detect the MS intensity of Bi and Pb in scintillation crystals of BGO and PWO. The rf-GD-MS experiments were carried out with the discharge pressure of 5.9 mPa and rf-power of 50 W. The MS intensity ^{209}Bi in BGO obtained was 1.00×10^{-14} without magnet, 6.25×10^{-12} for the single block, 1.74×10^{-11} for 2×2 magnet array, 2.77×10^{-11} for 3×2 magnet array and 2.37×10^{-11} for 3×4 magnet array. The MS intensity of ^{208}Pb in PWO obtained was 7.00×10^{-15} without magnet, 8.60×10^{-12} for the single block, 1.48×10^{-11} for 2×2 magnet array, 2.55×10^{-11} for 3×2 magnet array and 1.79×10^{-11} for 3×4 magnet array. The MS signal intensities for Bi with the three magnet arrays (2×2, 3×2 and 3×4) were 2.8, 4.4 and 3.8 times that of obtained with the single block magnet, and the MS signal intensities for Pb with the three arrays were 1.7, 2.9 and 2.1 times that of the single block magnet. Further, the MS signal intensities obtained with the magnet arrays were 630-3600 times that obtained in the absence of applied magnet, and an enhancement factor of 1.5-2.8 over that of the previously reported stacked magnetic device.[28]

Among the magnet array system, the signal enhancement observed for the 3 × 2 magnet array was superior to those of other arrays, which was consistent with the above simulation studies from COMSOL and the fuzzy synthetic evaluation result. The results further demonstrate that magnetic field distributions exert important

impacts on the signal intensity, and utilization of Larmor precession could effectively boost the ionization efficiency and increases signal intensity.

3.2.3 Stability Verification of the Magnet Array System with Typical Crystals

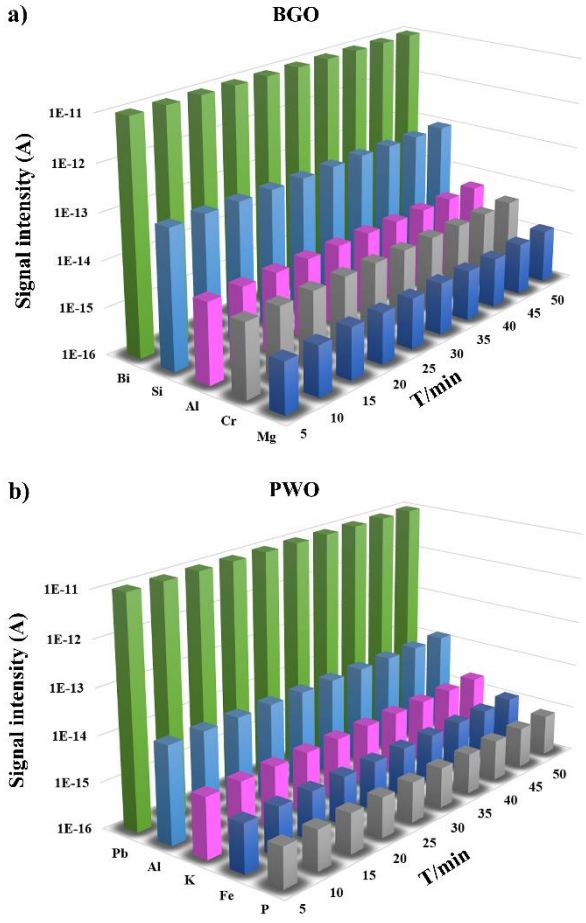

Figure 10. Stability of the discharge, represents by the signal intensity of the typical elements, as measured during sputtering of (a) BGO and (b) PWO by the 3×2 magnet array.

To verify the stability of magnet array system, signal intensities for typical elements in BGO and PWO samples were recorded at different sputtering time by rf-GD-MS with the 3×2 magnet array. Experiments were carried out with the discharge pressure of 5.9 mPa and rf-power of 50 W. The concentrations of ^{24}Mg, ^{27}Al, ^{28}Si and ^{52}Cr in BGO were analyzed as 2.72μg/g, 1.67μg/g, 170.74μg/g and 1.80μg/g respectively. The concentrations of ^{27}Al, ^{31}P, ^{39}K and ^{56}Fe in PWO were analyzed as $8.86\times10^3\mu$g/g, $1.14\times10^3\mu$g/g, $1.18\times10^3\mu$g/g and $6.61\times10^2\mu$g/g respectively. As shown in Figure 10, the relative standard deviation (RSD, n = 5) of the concentrations of typical elements in BGO and PWO were within 6.0 % and 11 %. Figure 10 further indicates that the discharge, sputtering, and ionization of each sample remained stable throughout the entire rf-GD-MS analysis process by the magnet array system.

3.2.4 Accuracy Verification of the Magnet Array System

Since the magnetic array system has been systematically investigated to distinctly enhance the MS signal intensity, the analytical accuracy and detection limits of the magnet array system with the 3×2 magnet array were also investigated. The standard samples NIST 611 and NIST 612 were used to calculate the sensitivities (RSF) and detection limits. The RSF of elements, including ^{75}As, ^{52}Cr, ^{208}Pb, ^{24}Mg, ^{58}Ni, ^{85}Rb, ^{88}Sr, ^{232}Th, ^{238}U, and ^{48}Ti, were calculated by determining the ratio of the certified concentration to the measured concentration. The measured RSF values for the selected elements are listed in Table 2.

Table 2. Measured Concentrations, RSF, and Detection Limits for the Elements in the NIST 611 (Relative to Si)

elements	certified concentration C_0 (μg/g)	measured concentration C (μg/g)	RSF (C_0/C)	detection limit (μg/g)
^{75}As	340	296.10	1.15	0.33
^{52}Cr	415	471.23	0.88	0.63
^{208}Pb	426	746.73	0.57	0.86
^{24}Mg	457	295.46	1.55	0.0032
^{58}Ni	458	508.57	0.90	0.23
^{85}Rb	425.7	829.77	0.51	0.98
^{88}Sr	515.5	921.45	0.56	0.0038
^{232}Th	457.2	696.20	0.66	0.91
^{238}U	461.5	701.85	0.66	0.45
^{48}Ti	437	747.13	0.58	0.020

In most cases, the detection limit (DL) was calculated with the following formula:

$$\text{Detection Limit} = 3\sigma_B/s \quad (7)$$

In Eq 7, σ_B represents the blank noise and s represents the calibration curve slope. Analytical methods with high sensitivity and fairly low noise should give low DLs. The DLs are presented in Table 2 and the DL of the 3×2 magnet array rf-GD-MS analysis method can reach 0.0032μg/g while that from the single block magnet was 0.056μg/g and from the previous stacked magnets was 0.0082μg/g. Moreover, the low DL for analysis of trace elements can improve the performance of rf-GD-MS detection methods.

The RSF values in Table 2 were used to measure the element concentrations in the NIST 612 sample. Then the relative detection error was calculated by comparing the certified concentrations and the RSF-calibrated concentrations. Table 3 shows that relative errors for the elements ranged from 0.16−9.97 %, thus the accuracy of the magnet array enhanced method was verified.

Table 3. Comparison of rf-GD-MS Results for NIST 612 Calibrated by RSF and the Certified Concentration (Relative to Si)

elements	certified concentration C_0 (μg/g)	measured concentration C (μg/g)	calibrated concentration by RSF (μg/g)	relative error (%)
^{75}As	37.4	32.75	37.61	0.55

^{52}Cr	35.0	39.68	34.95	-0.16
^{208}Pb	38.57	66.32	37.83	-1.91
^{24}Mg	37.7	23.44	36.26	-3.83
^{58}Ni	51	43.20	45.14	2.06
^{85}Rb	31.4	60.39	30.98	-1.33
^{88}Sr	78.4	128.38	71.89	-8.30
^{232}Th	37.79	51.81	34.02	-9.97
^{238}U	37.78	61.40	40.37	8.01
^{48}Ti	50.1	88.87	51.98	3.75

CONCLUSION

In our present work, the mechanism of signal enhancement of the magnet array system was demonstrated by COMSOL studies. The results suggested that the magnet arrays display clear oscillating magnetic field distributions, and the trajectories of electrons motions were curved and prolonged by the oscillating magnetic field into spirals to conduct Larmor precession. Moreover, Larmor precession resulted in numerous secondary electrons from the inelastic collisions between primary electrons and samples, which could lead to more collisions between electrons and other particles and further boosted the ionization efficiency. The fuzzy synthetic evaluation results also indicated that the 3×2 magnet array device displayed the most significant enhancement among the four magnet array devices.

With the guidance of the theoretical studies, a magnet array system with four magnetic devices of single block and 2×2, 3×2, and 3×4 magnet arrays was constructed and applied to analyze BGO and PWO crystals. The signal enhancement observed for the 3×2 array was superior to those of other magnet arrays, which was consistent with the simulation studies from COMSOL and the fuzzy synthetic evaluation result. The signal intensities obtained for ^{209}Bi and ^{208}Pb were improved by factors of 4.4 and 2.9 with the 3×2 magnet array, as compared to methods using transverse block magnet. The accuracy and detection limits for the magnet array method were verified with NIST samples 611 and 612. The relative errors were calculated to be less than 10 % and the lowest detection limit reached 0.0032μg/g. The results show that the magnet array enhancement system features a prospective manner for the efficient analysis of nonconducting materials by rf-GD-MS. Further studies in this area are being carried out in our laboratory.

AUTHOR INFORMATION

Corresponding Author

* E-mail: qianrong@mail.sic.ac.cn. Phone: +862169163655. Fax: +862169163783.

ORCID

Rong Qian: 0000-0002-4732-5553

Author Contributions

The manuscript was written through contributions of all authors. All authors have given approval to the final version of the manuscript.

Notes

The authors declare no competing financial interest.

ACKNOWLEDGMENT

The authors greatly acknowledge the financial support by the National Natural Science Foundation of China (Grant No. 21775156) and the Intergovernmental International Cooperation Project of Shanghai Science and Technology Commission (Grant No. 19520712000).

REFERENCES

(1) Fu, J.; Yu, P.; Zhang, N.; Ren, G.; Zheng, S.; Huang, W.; Long, X.; Li, H.; Liu X. *Energy Environ. Sci.*, **2019**, *12*, 1404-1412.
(2) Lahmer, M. A. *Appl. Surf. Sci*. **2018**, *457*, 315–322.
(3) Quarles, C. D.; Castro J.; Marcus, R. K. *Glow Discharge Mass Spectrometry in: Encyclopedia of Spectroscopy and Spectrometry*, 3rd ed., Amsterdam: Elsevier Ltd. **2017**, 30-36.
(4) Paudel G.; Kasikb M.; Sabatinoa M. D. *J. Anal. At. Spectrom*. **2019**, *34*, 1829–1837.
(5) Brackmann, V.; Hoffmann, V.; Kauffmann, A.; Helth, A.; Thomas, J.; Wendrock, H.; Freudenberger, J.; Gemming, T.; Eckert, J. *Mater. Charact.* **2014**, *91*, 76–88.
(6) Pisonero, J.; Feldmann, I.; Bordel, N.; Sanz-Medel, A.; Jakubowski, N. *Anal. Bioanal. Chem.* **2005**, *382*, 1965–1974.
(7) Evans, E. H.; Pisonero, J.; Smith, C. M. M.; Taylor, R. N. *J. Anal. At. Spectrom*. **2014**, *29,* 773–794.
(8) Plotnikov A.; Pfeifer J.; Richter S.; Kipphardt H.; Hoffmann V. *Anal. Bioanal. Chem*. **2014**, *406*, 7463–7471.
(9) Voronov M.; Šmíd P.; Hoffmann V.; Hofmanna T.; Venzago C. *J. Anal. At. Spectrom*. **2010**, *25*, 511–518.
(10) Hang, L.; Xu, Z.; Yin, Z.; Hang, W. *Anal. Chem*. **2018**, *90*, 13222-13228.
(11) Gonzalez-Gago, C.; Smid, P.; Hofmann, T.; Venzago, C.; Hoffmann, V.; Gruner, W. *Anal. Bioanal. Chem.* **2014**, *406*, 7473–7482.
(12) Gubal, A; Ganeev, A.; Hoffmann, V.; Voronov, M.; Brackmann, V.; Oswald, S. *J. Anal. At. Spectrom.* **2017**, *32*, 354-366.
(13) Dong, J.; Qian, R.; Zhuo, S.; Yu, P.; Chen, Q.; Li Z. *J. Anal. At. Spectrom.* **2019**, *34*, 2244–2251.
(14) Pisonero J.; Valledor R.; Licciardello A.; Quirós C.; Martín J. I.; Sanz-Medel A.; Bordel N. *Anal. Bioanal. Chem.* **2012**, *403*, 2437–2448.
(15) Shick, C. R.; DePalma, P. A.; Marcus, R. K. *Anal. Chem.* **1996**, *68*, 2113–2121.
(16) Giglio, J. J.; Caruso, J. A. *Appl. Spectrosc.* **1995**, *49*, 900–906.
(17) Vega, P.; Valledor, R.; Pisonero, J.; Bordel, N. *J. Anal. At. Spectrom.* **2012**, *27*, 1658–1666.
(18) Voronov, M.; Hoffmann, V.; Buscher, W.; Engelhard, C.; Rayc, S. J.; Hieftje, G. M. *J. Anal. At. Spectrom.* **2011**, *26*, 811–815.
(19) Bouza, M.; Pereiro, R.; Bordel N.; Sanz-Medela, A.; Fernandez, B. *J. Anal. At. Spectrom.* **2015**, *30*, 1108–1116.
(20) Bodnar, V.; Ganeev, A.; Gubal, A.; Solovyev, N.; Glumov, O.; Yakobson, V.; Murin, I. *Spectrochim. Acta, Part B.* **2018**, *145*, 20-28.
(21) Fernandez, B.; Lobo, L.; Tyagi, P.; Stoichkov, V.; Kettle, J.; Pereiro, R. *Talanta* **2019**, *192*, 317.
(22) Winchester, M. R.; Payling, R. *Spectrochimica Acta Part B*. **2004**, 59, 607–666.
(23) Bentz, B. L.; Harrison, W. W. *Anal. Chem.* **1982**, *54*, 1644-1646.
(24) Chen, M.; Ren, J.; Ma, H.; Zhang, G. *Spectrochim. Acta, Part B* **1997**, *52*, 1161-1166.
(25) Heintz, M.J.; Broekaert, J.A.C.; Hieftje, G. M. *Spectrochim. Acta, Part B* **1997**, *52*, 579–591.
(26) Saprykin, A. I.; Becker J. S.; Dietze, H.-J. Fresenius´ J. *Anal. Chem.* **1997**, 359, 449–453.
(27) Vega, P.; Pisonero, J.; Bordel, N.; Tempez, A.; Ganciu, M.; Sanz-Medel, A. *Anal. Bioanal. Chem.* **2009**, *394*, 373–82.

(28) Wei, J.; Dong, J.; Zhuo, S.; Qian, R.; Fang, Y.; Chen, Q.; Patel, E. *Anal. Chem.* **2017**, *89*, 1382–1388.
(29) Dolker, E. M.; Petkovic, B.; Schmidt, R.; Ziolkowski, M.; Brauer, H.; Haueisen, J. *Compel-Int. J. Comp. Math. Electr. Electron. Eng.* **2019**, *38*, 943–952.
(30) Belykh, V. V.; Yakovlev, D. R.; Bayer M. *Phy. Rev. B* **2019**, *99*, 161205(R).
(31) Zhukov, E. A.; Kirstein, E.; Kopteva, N. E.; Heisterkamp, F.; Yugova, I. A.; Korenev, V. L.; Yakovlev, D. R.; Pawlis, A.; Bayer, M.; Greilich, A. *Nat. Commun.* **2018**, *9*, 1941.
(32) Saelens, W.; Cannoodt, R.; Saeys, Y. *Nat. Commun.* **2018**, *9*, 1090.

TOC Graphic